NUMERICAL STUDIES ON SIMULATIONS OF WAVES AND NEARSHORE CURRENTS IN NON-ORTHOGONAL MESH SYSTEM

Yan DING

Research Scientist, National Center for Computational Hydroscience and Engineering,
The University of Mississippi, University, MS 38677-1848, U.S.A. Email:ding@ncche.olemiss.edu

Sam S. Y. WANG

FAP Barnard Distinguished Professor and Director, Same Institute

Yafei JIA
Research Associate Professor, Same Institute

Abstract: In the paper, process-based models for simulating irregular wave deformation and nearshore currents are developed. The numerical models are based on a non-orthogonal mesh system so that the models are capable of solving coastal process problems combined with waves and currents in complex shorelines. The wave model, which is based on a multi-directional spectral energy balance equation, is validated through simulations of wave heights over an elliptical shoal, for which the Bretschneider-Mitsuyasu spectrum and the TMA spectrum are employed. The current model for computing the nearshore currents in an experimental wave basin is further tested. The computed currents under the attacks of oblique incident waves are in good agreement with the measured data.

Key words: Irregular wave estimation, Nearshore current, Coastal processes, Non-orthogona coordinates

1. INTRODUCTION

A goal of estimation of wave fields and wave-driven nearshore currents is to understand the evolution of random waves propagating across the nearshore to the beach, the corresponding nearshore currents, and the subsequent evolution of morphology in coastal zones. Calculations of the representative wave heights of irregular waves and predictions of the nearshore currents play a crucial role in management and protection of coastlines, designs of coastal structures, and environmental assessments in coastal zones. The special purpose of the numerical studies is to develop an integrated application package for simulations and predictions of irregular waves and nearshore currents. A multi-directional spectral wave transformation model that can effectively describe the random wave transformation and wave breaking from deepwater offshore to shallow water nearshore is used for computing the spatial distribution of the significant wave heights and periods. The two-dimensional shallow water equations are adopted for simulations of nearshore currents by considering the radiation stress due to wave actions. However, because of irregularly shaped shorelines, a non-orthogonal mesh system proposed by Jia and Wang (1999) is used for handling complex geometries in coastal zones. The present model is validated on computing irregular wave over an elliptical shoal built in a laboratory flume by Vincent and Briggs (1989). By comparing the computed wave heights and currents with the measurements taken by Visser (1991), the validation of nearshore currents model is achieved on simulations of nearshore currents

induced by oblique incident wave actions in a wave basin. The eddy viscosity models included in the nearshore current model are also discussed. Numerical results show that the process-based models are capable of evaluating irregular waves and nearshore currents in coastal zones with complex geometries.

2. MATHEMATICAL MODELS FOR WAVES AND CURRENTS

2.1 MULTI-DIRECTIONAL SPECTRAL WAVE TRANSFORMATION MODEL

In the modeling of irregular wave deformation from offshore to onshore, the spectral energy balance equation proposed by Karlsson (1969) is employed. The variations of wave energy density $S(x,y,\theta,f)$ under the attack of multi-directional incident waves can be written as

$$\frac{\partial Sv_x}{\partial x} + \frac{\partial Sv_y}{\partial y} + \frac{\partial Sv_\theta}{\partial \theta} = Q ,$$
(1)

where θ=the wave direction; x, y=spatial coordinates; Q=a source term generated by energy dissipation due to wave breaking and bottom friction; v= the energy transport velocity,

i.e. $v_x = C_g \cos\theta, \quad v_y = C_g \sin\theta, \quad v_\theta = \frac{C_g}{C}\left(\sin\theta \frac{\partial C}{\partial x} - \cos\theta \frac{\partial C}{\partial y} \right),$
(2)

where C=wave celerity; Cg=wave group celerity. The directional spread of the wave energy is frequency dependent, so the directional formulations are commonly defined as

$$S(f,\theta) = S(f)D(f,\theta) ,$$
(3)

in which $S(f)$ = a one-dimensional frequency spectrum; $D(f,\theta)$ = a directional spreading function. A number of the one-dimensional wave spectra models can be found in the literature. Hereafter, the Bretschneider-Mitsuyasu (B-M) spectrum (Mitsuyasu 1970) and the TMA spectrum (Bouws et al. 1985) are used for simulating the irregular wave deformation. The Goda's wave breaking criterion is included in the model by introducing a dissipation term into the right-hand side of (1). For the details of this term, see Takayama et al. (1991).**2.2 NEARSHORE CURRENT MODEL**

The nearshore current is basically governed by the shallow water equations including the additional radiation stress, namely

$$\frac{\partial \eta}{\partial t} + \nabla \cdot (h\mathbf{u}) = 0 ,$$
(4)

$$\frac{\partial \mathbf{u}}{\partial t} + \mathbf{u}\cdot\nabla \mathbf{u} = -g\nabla\eta + \frac{1}{h}\nabla\cdot(hf) - \frac{\nabla\cdot R}{h} - \frac{f^b}{\rho h} ,$$
(5)

where η = water elevation; h = water depth; $\mathbf{u}$ = the depth averaged velocity vector in two horizontal directions; g=the gravitational acceleration; ρ=water density; R=the wave-induced radiation stress; τ^b=the bottom friction stress. The wave-induced radiation stress tensor can be derived under the assumption of small-amplitude waves (Longuet-Higgins and Stewart 1963). In (5) the depth-averaged Reynolds stress τ can be represented as a model of turbulence closure. The present nearshore current model provides users with the following two zero-equation models. One is the Longuet-Higgins eddy viscosity model (Longuet-Higgins 1970), by which the eddy viscosity v_e is written as

$$v_e = Nl\sqrt{gh} ,$$
(6)

where N=empirical coefficient (=0.001-0.01); l = the distance from shoreline toward offshore. Another model is the Larson-Kraus eddy viscosity model (Larson & Kraus 1991), i.e.

$$v_e = \Lambda U_W H ,$$
(7)

where Λ=empirical coefficient (=0.1-3.0); U_W=the magnitude of wave orbital velocity at the upper limit of the bottom boundary layer; H=wave height. The bottom friction stress τ^b can be represented as a time-averaged combination of wave and mean current, namely

$$\tau^b = \rho C_f \sqrt{\mathbf{u} + \mathbf{u}_b \mid (\mathbf{u} + \mathbf{u}_b)} ,\tag{8}$$

where the overbar means the time-averaged integration over a wave period; C_f = friction coefficient; $\mathbf{u}_b$=the wave orbital velocity at the bottom. The friction law of the combined wave and current proposed by Tanaka and Thu (1994) is used to estimate the friction coefficient in the different flow regimes, including rough turbulent flow, smooth turbulent flow, and laminar flow. The combined friction coefficient f_{cw} (=$2C_f$) is given as follows,

$$f_{cw} = f_c + 2\sqrt{f_c \beta f_w} \mid \cos\phi \mid + \beta f_w ,\tag{8}$$

where f_c, f_w = the friction coefficients due to mean current and wave, respectively; β=the coefficient due to nonlinear interaction of waves and currents; ϕ= the angle between wave orthogonal and current vector. One may refer to Tanaka and Thu (1994) for the details of calculating the friction coefficients in different flow regimes.

3. NUMERICAL APPROACHES

At first the energy balance equation (1) about the irregular wave deformation was solved by means of the parabolic approximation. The waves were assumed to have a principal propagation direction (say x which direction is from offshore to onshore), and then the calculation of the waves was therefore carried out from offshore to onshore. In this study, the reflection effect of the waves in the negative x-direction was assumed to be negligible. Sequentially, a special finite element method called the Efficient Element Method (EEM) (Jia and Wang 1999) was used for computing the wave-induced currents by including the radiation stress. Using this numerical technique, a collocation approach based on the Lagrangian interpolation functions was adopted to discretize the governing equations. A quadrilateral with nine nodes was used to form an element of velocity in a two-dimensional domain. The quadrilateral for an element of water level was defined at the staggered location to the velocity element. The model was designed for non-orthogonal grid systems; it was therefore capable of simulating waves and currents in a coastal zone with a complex coastline. In the model, a velocity correction method was used to decouple the continuity equation (4) and the momentum equations (5); the upwinding scheme is used to construct the convective operator. For more details about the numerical techniques, one may refer to Jia and Wang (1999) and Jia et al. (2002).

4. NUMERICAL RESULTS

4.1 IRREGULAR WAVE DEFORMATION OVER AN ELLIPTICAL SHOAL

In order to validate the multi-directional spectral wave model, we computed the distributions of irregular waves over an elliptical shoal. The elliptical shoal in an experimental flume built by Vincent and Briggs (1989) had a major radius of 3.96m, a minor radius of 3.05m, and a maximum height of 30.48cm at the center. The region outside the shoal was of constant depth (45.72cm). Using a directional spectral wave generator, Vincent and Briggs (1989) produced irregular wave conditions, and measured wave heights along several sections in several cases with different wave spectra. In their experiments, the incident irregular wave spectrum was described by the TMA spectrum (Bouws et al. 1985), and the mean wave direction is identical to the axis of the minor radius. For the validation purpose, we only considered two cases with different directional spreading spectra of their total seventeen test cases investigated by Vincent and Briggs (1989). One was the narrow directional spreading spectrum (Case N1); another was the broad directional spreading spectrum (Case B1). The

input parameters of the TMA spectra are shown in Table 1, in which the H_0 is the incident significant wave height, T_0 is the period of wave, α is the alpha constant, γ is the peak enhancement factor, and σ_m is the directional spreading parameter. A Fourier series representation for the wrapped normal spreading function was used in the TMA spectrum (Vincent and Briggs 1989), and then fifty harmonics were chosen to represent the directional spreading function $D(f, \theta)$. The B-M spectrum was also used for comparing the performance of different spectra. Therefore, the selected values of S_{max} in the B-M spectra, which represent the directional spreading (Mitsuyasu et al. 1975), are shown in Table 1. In the computations of the wave fields, the lower and upper frequency limits were respectively 0.5Hz and 10Hz. $\Delta f=0.095$ (101 frequency bins) and $\Delta\theta=5.0^O$ (37 directional bins between -90° and $+90^O$) were used. The spatial increments $\Delta x=\Delta y=10cm$ were used to create a uniform mesh. The distributions of the normalized significant wave heights (Hs/H_0) in Case N1 and B1, which were computed by means of the B-M spectra, are shown in Fig. 1(a) and Fig. 1(b), respectively. The wave rays shown in the figures represent the mean directions of wave propagations. The waves generated by the narrow directional spreading spectrum (Case N1) show a stronger convergence region behind the shoal than that by the broad directional spreading spectrum (Case B1). In Fig. 2, the normalized wave heights along four different transects obtained by the TMA and the B-M spectra in the two cases are compared with the corresponding measured wave heights. The numerical results in Fig. 2 show that both the TMA and the B-M spectra can predict very accurate wave heights, which are in good agreement with the measurements. However, since the diffraction is not included in the energy balance equation (1), this effect behind the shoal may need to be further studied.

Table 1 Input data of wave spectra for test cases

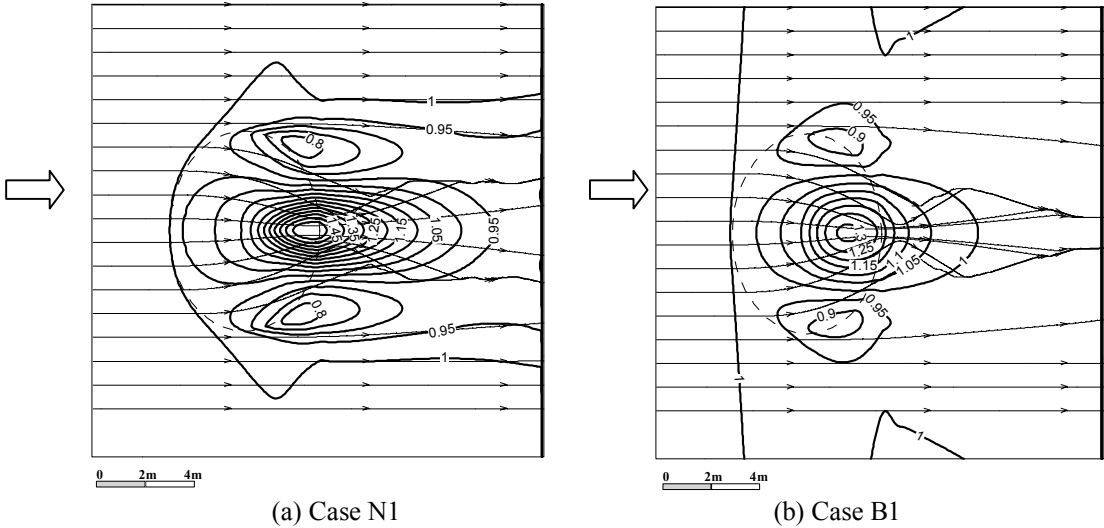| Case No.	H_0 (cm)	T_0 (s)	α	γ	σ_m (deg)	S_{max}
N1	7.75	1.30	0.01440	2	10	75
B1	7.75	1.30	0.01440	2	30	10

(a) Case N1 (b) Case B1

Fig. 1 Normalized wave heights (Hs/H_0) and wave rays for narrow and broad directional spreading (the dashed line on the figures represents the outline of the elliptical shoal)

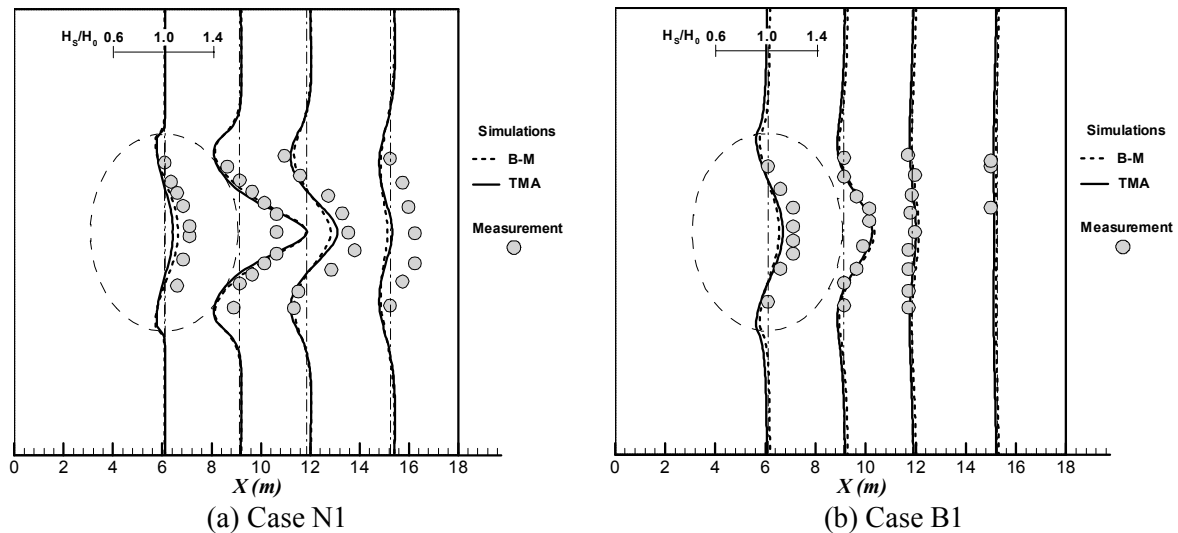(a) Case N1   (b) Case B1

Fig. 2 Comparisons of normalized wave heights between computations and measurements (The dashed dot lines represent the locations of measurement transacts)

4.2 UNIFORM LONGSHORE CURRENTS

When waves break obliquely to the shoreline a mean current is generated flowing parallel to the coastline. Visser (1991) performed the experiments on uniform longshore/nearshore currents in a wave basin with a pumped recirculation through opening in the wave-guide walls. The experimental wave basin was 34.00m long, 16.60m wide and 0.68m deep. Concrete beaches with uniform slopes 1:10 and 1:20 were constructed toward shoreline so that the depth contours in the basin were parallel to the straight shoreline. The wave guide-walls were installed obliquely at an angle of $15.4°$ with the normal to the wave board. For the validations of the longshore current produced in the experiments, a quadrilateral mesh was generated over the parallelogram-like wave basin. The two cases of the experiments, of which the incident wave heights and oblique wave angles α are shown in Table 2, were carried out by the present model. In particular, the two cases have two different foreshore slope β (1:20 and 1:10), different recirculation flow rate Q_p and still water depth d. Here the B-M spectra were used for computations of wave deformation. Because the regular incident waves were generated in the experiments, a large value of S_{max} (=90) was used so that the B-M multi-directional wave spectrum was still capable of simulating the cases with regular waves. Fig. 3 shows the computed wave heights and wave directions of Case 1 in which the mesh detail near the shoreline is shown in the upper left corner. The computed wave heights and wave angles are compared with measurements in Fig. 4 (a) and (b), respectively. Good agreements between the computations and the measurements of waves are obtained. The computed longshore currents and streamlines are shown in Fig. 5 (a). It is obvious that the computed flow pattern consists of the longshore current, the internal recirculation, and an induced recirculation at the upper right corner. In the experiments, the inflows in the opening of the updrift wave guide were pumped from the opening in the downstream wave guide. Therefore in the computations the pumped flow rates are specified as inflow rates at the inlet (opening) boundary. The downstream opening in the computations was set as an outlet boundary, and the width of the opening was kept the same as that in the experiments. The friction coefficient C_f calculated by the friction law of the combined wave and current in (8) is shown in Fig. 5 (b). The variation of the friction coefficient is from 0.004-0.04; and the value of C_f is approximately 0.008 in the surf zone which is very close to the value (C_f=0.007) calibrated by Larson and Kraus (1991). Moreover, the computed profiles of the longshore currents at Sections 2 and 3 of which the locations are shown in Fig. 3 are compared with these measured velocities in Fig. 6 (a) and (b), respectively. In computations for Case 1, two eddy viscosity models with the optimal

empirical coefficient values, i.e. the Longuet-Higgins formulation (6) in which $N=0.002$, and the Larson-Kraus formulation (7) in which $\Lambda=1.0$, were used. The comparisons of the currents show that the predictions by the former eddy viscosity formulation are much better than those by the latter, and the latter model even generated an unrealistic high-speed current near the side of wave generator. Because of the fact that the flow of the longshore current was a type of boundary layer flow, the Longuet-Higgins model based on the mixing length theory can predict the currents more accurately than the latter model. The Longuet-Higgins model with the calibrated value of N was then used to predict the currents in Case 2 in which the foreshore slope (1:10) is steeper than Case 1. The comparisons of the currents in Case 2 at sections 2 and 3 are given in Fig. 7. It shows that the computed longshore currents in sections 2 and 3 agree with their measurements very well. Because of the steeper foreshore slope in Case 2, the wave breaking line is closer to shoreline, and the width of the longshore current in Case 2 becomes narrower than Case 1.

Table 2 Input data of wave spectra, foreshore slope β and flow conditions for test cases

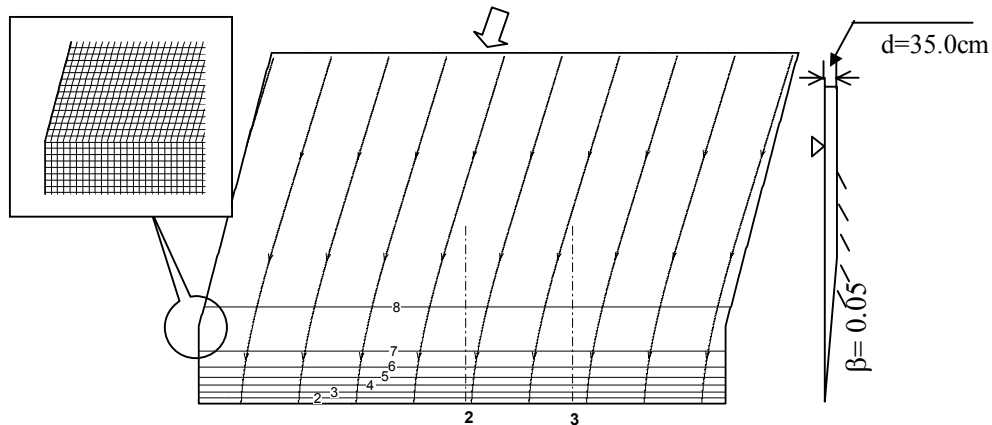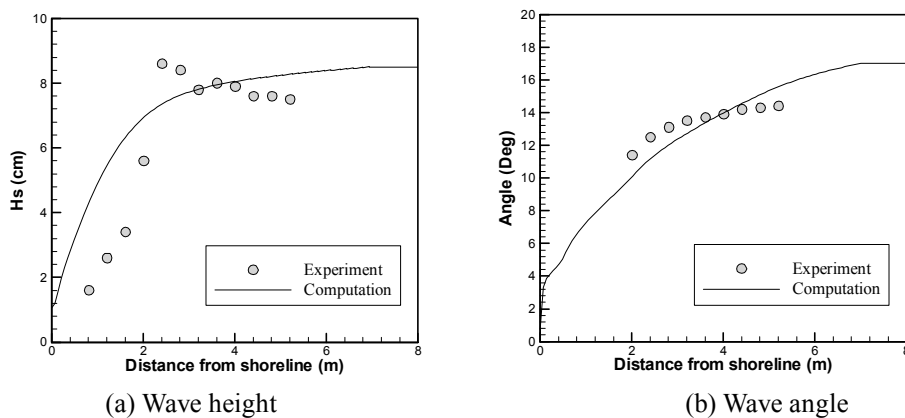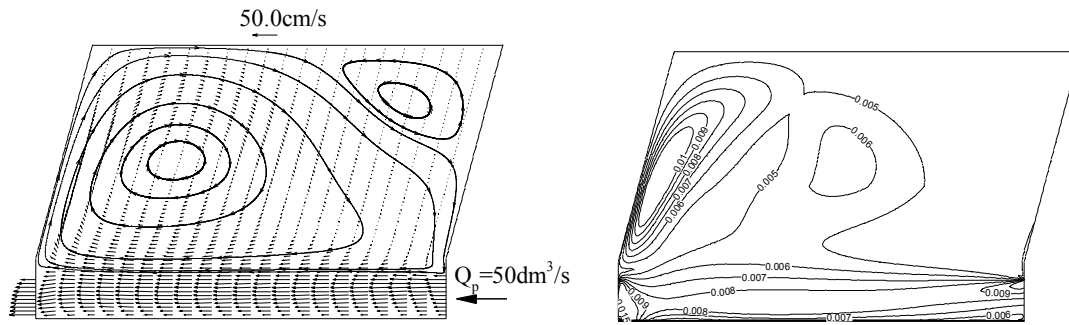| Case No.	H_0 (cm)	T_0 (s)	α (deg)	β	Q_p (dm³/s)	d (cm)
1	8.5	1.02	17.0	0.05	50.0	35.0
2	9.6	1.00	16.4	0.101	40.0	40.1

Fig. 3 Significant wave height (cm) and wave rays in Case 1 (The figure at the corner shows the close-up of mesh near shoreline. The dashed dot lines represent the sections of measurements)
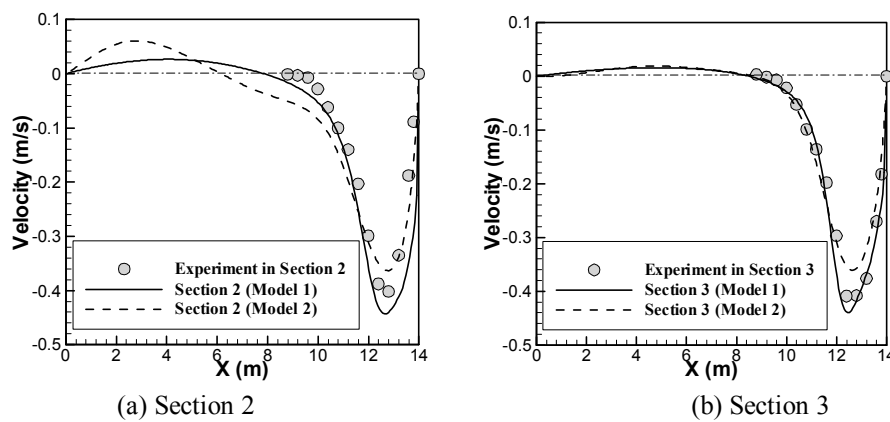

(a) Wave height　　　　　　　　　(b) Wave angle
Fig. 4 Comparisons of wave heights and wave angles in Case 1

(a) Currents   (b) Friction coefficients C_f

Fig. 5 (a) Computed current vectors and streamlines in Case 1, and (b) Friction coefficient C_f calculated by the friction law under combined wave and current

(a) Section 2   (b) Section 3

Fig. 6 Comparisons of profiles of longshore currents between computations and measurements at two sections in Case 1 (Model 1: Longuet-Higgins Model, N=0.002; Model 2:Larson-Kraus Model, Λ=1.0)
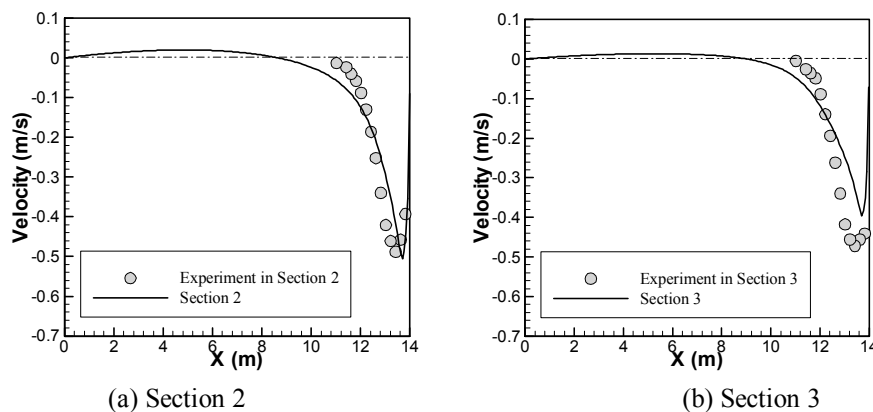
(a) Section 2   (b) Section 3

Fig. 7 Comparisons of profiles of longshore currents between computations and measurements at two sections in Case 2 (Eddy viscosity model: Longuet-Higgins Model, N=0.002)

5. CONCLUSIONS

In the study, process-based models for predicting irregular waves and nearshore currents were developed. The numerical models are based on a non-orthogonal mesh system so that the models are capable of predicting the coastal processes combined with waves and currents in a complex shoreline. The model for predicting the irregular waves was validated through simulations of wave heights over an elliptical shoal, for which the two spectra of irregular waves, i.e. the B-M spectrum and the TMA spectrum, were employed. The obtained results

indicate that the performances of the two spectra are quite comparable. Moreover, the model for computing the nearshore currents in an experimental wave basin was further tested. The computed currents generated by different obliquely incident waves are in good agreement with their measured ones. Comparisons of the numerical and measured currents show that the type of mixing length model can predict the longshore currents more accurately than the model based on the wave height and its orbital velocity. The simulations of the nearshore currents with different bed slopes are also achieved. In the future, we will address the studies of modeling sediment transport under combinations of waves and currents to construct an integrated model of coastal processes.

ACKNOWLEDGEMENTS

REFERENCES
Bouws, E., Gunther, H., Rosenthal, W., and Vincent C. L. (1985). "Similarity of the wind wave spectrum in finite depth water, 1-Spectral form." *J. Geophys. Res.,* 90(C1), 975-986.

Jia, Y., and Wang, S. S. Y. (1999). "Numerical model for channel flow and morphological change studies." *J. Hydr. Engrg.*, ASCE, 125(9), pp924-933.

Jia, Y., Wang, S. S. Y., and Xu, Y. C. (2002), "Validation and application of a 2D model to channel with complex geometry." *Int. J. Computational Engineering Science*, 3(1), 57-71.

Karlsson, T. (1969). "Refraction of continuous ocean wave spectra." *J. Waterways and Harbors Division*, Proc. ASCE, Vol. 95, No. WW4, 437-447.

Larson, M., and Kraus, N. C. (1991). "Numerical model of longshore current for bar and trough beaches." *J. Wtrway., Port, Coast. and Oc. Engrg.,* ASCE, 117(4), 326-347.

Longuet-Higgins, M.S., and Stewart, R.W. (1963). "Radiation stress and mass transport in gravity waves with application to surf beats." *J. Fluid Mech.,* 13, 481-504.

Longuet-Higgins, M. S. (1970). "Longshore currents generated by obliquely incident wave." *J. Geophys. Res.,* 75(33), 6778-6789.

Mitsuyasu, H. (1970). "On the growth of spectrum of wind-generated waves (2) – spectral shapes of wind waves at finite fetch -." *Proc. 17th Japanese Conf. on Coastal Engrg.*, pp. 1-7 (in Japanese)

Mitsuyasu, H., Tasai, F., Subara, T., Mizuno, S., Ohkusu, M., Honda, T., and Rikiishi, K. (1975). "Observations of the directional spectrum of ocean waves using a clover-leaf buoy." *J. Phys. Oceanogr.*, 5, 750-760.

Takayama, T., Ikeda N., and Hiraishi, T. (1991). "Practical computation method of directional random wave transformation", *Report of Port and Harbour Res. Inst.*, Vol. 30, No.1, 22-67 (in Japanese)

Tanaka, H., and Thu, A. (1994). "Full-range equation of friction coefficient and phrase difference in a wave-current boundary layer." *Coastal Engineering*, Vol. 22, 237-254.

Vincent, C. L., and Briggs, M. J. (1989). "Refraction-difraction of irregular waves over a mound." *J. Wtrway., Port, Coast. and Oc. Engrg.,* ASCE, 115(2), 269-284.

Visser, P. J. (1991). "Laboratory measurements of uniform longshore currents." *Coastal Engineering*, 15(5), 563-593.